

A Lattice QCD study of $p - \Lambda$ scattering in continuum and chiral limits

Hang Liu,¹ Liuming Liu,² Jin-Xin Tan,³ Wei Wang,^{3,4} Haobo Yan,⁵ and Qian-Teng Zhu³

¹*Department of Physics, Shanghai Normal University, Shanghai 200234, China*

²*Institute of Modern Physics, Chinese Academy of Sciences, Lanzhou, Gansu Province 730000, China*

³*INPAC, Key Laboratory for Particle Astrophysics and Cosmology (MOE),*

Shanghai Key Laboratory for Particle Physics and Cosmology,

School of Physics and Astronomy, Shanghai Jiao Tong University, Shanghai 200240, China

⁴*Southern Center for Nuclear-Science Theory (SCNT), Institute of Modern Physics, Chinese Academy of Sciences, Huizhou 516000, Guangdong Province, China*

⁵*School of Physics, Peking University, Beijing 100871, China*

We present a first systematic study of $I = 1/2$ proton- Λ ($p - \Lambda$) scattering from lattice QCD, using seven sets of $(2+1)$ -flavor lattice ensembles with pion masses spanning 135–317 MeV and three lattice spacings with $a = (0.052, 0.077, 0.105)$ fm. Using Lüscher’s finite-volume method, effective range expansion and chiral/continuum extrapolations, we obtain the inverse of scattering length and effective range for the 1S_0 channel as 0.177(83) GeV and 2.9(1.4) fm, and for the 3S_1 channel as 0.016(76) GeV and 1.8(1.1) fm. From the derived S-wave phase shifts, we provide an estimate of the $p - \Lambda$ scattering cross section. Our results for scattering length, effective range and cross sections are in good agreement with available experimental measurements. We also find that the $p - \Lambda$ system sustains attractive interactions. These results provide critical input for the unification of nuclear force theories and the construction of neutron star equations of state.

Introduction: Nucleon- Λ scattering serves as an indispensable probe of strangeness $S = -1$ baryon-baryon dynamics, bridging the non-strange (nucleon) and strange (Λ hyperon) sectors to address foundational questions across nuclear physics, astrophysics, and QCD. Its importance extends from constraining the Λ single-particle potential in hypernuclei [1]—critical for unraveling the role of strangeness in nuclear matter—to resolving the “hyperon puzzle” in neutron stars [2–4]: the tension between predicted hyperon-induced softening of the equation of state (EoS) and observations of massive neutron stars $M > 1.97M_\odot$ [5, 6]. Furthermore, $p - \Lambda$ scattering data is critical for developing a unified theory of nuclear forces [7], as it tests flavor symmetry breaking and non-perturbative QCD effects that elude direct computation.

On the experimental front, while early measurements of $p - \Lambda$ scattering cross sections date back to 1960s [8], including a range of investigations in both low- and high-energy regimes [9–15], several important progress have made recently. CLAS collaboration reported a high-precision measurement of the $p\Lambda \rightarrow p\Lambda$ cross section between 0.9 and 2.0 GeV/c based on modern technologies [16], while BESIII collaboration has used the beam pipe that contains the proton and the Λ from $J/\psi \rightarrow \Lambda\bar{\Lambda}$ and reported their measurement of the $p\Lambda \rightarrow p\Lambda$ scattering at a Λ momentum of 1.074 GeV/c [17]. Using the data on two-particle correlations in $\sqrt{s_{NN}} = 3\text{GeV}$ Au+Au collisions from STAR, Ref. [18] has presented preliminary results on scattering length and effective range of $p - \Lambda$. Altogether, these recent high-precision results lay a solid experimental foundation for quantitative and precision studies of the $p\Lambda$ interaction system.

From the theoretical aspect, understanding $p - \Lambda$ interactions has been hindered by the long-standing limitations in theoretical calculations. Phenomenological models, such as meson-exchange potentials [19–26], con-

stituent quark models [27, 28] and Bethe-Salpeter approach [29], relied on adjustable parameters, leading to large uncertain predictions for in key observables like scattering lengths and effective ranges. While chiral effective field theory (χ EFT) provides a systematic approach [1, 30–35], its predictions depend on low-energy constants (LECs) calibrated to imprecise experimental data [16, 36], resulting in less-precise constraints on the $p - \Lambda$ potential strength. Early lattice QCD studies, were constrained by quenched approximations [37] or limited to unphysical pion masses ($m_\pi \gg 135$ MeV) on a coarse lattice [38–44], making extrapolation to the physical point prone to systematic errors. These theoretical ambiguities have propagated to downstream applications: models of neutron star EoS remain fragmented [45], and the role of three-body forces in hypernuclei remains unresolvable [46].

To overcome these barriers, a precise lattice QCD calculation at the physical pion mass and in the continuum limit is imperative. In response to this demand, in this work, we present a systematic lattice QCD study of the $p - \Lambda$ interaction using the Lüscher finite-volume method, which relates the energy spectrum in a finite volume to infinite-volume scattering parameters. Our calculations employ seven ensembles with three lattice spacings and various pion masses ranging from 135MeV to 317MeV, enabling a controlled extrapolation to the physical pion mass and continuum limit. For the first time, we report the scattering lengths and effective ranges for both the 1S_0 and 3S_1 channels at the physical pion mass and continuum limit, results that can be directly compared with experimental measurements. These results do not merely supplement the existing literature, they fill the critical gap in hyperon-nucleon interaction data, providing useful inputs to help resolve the hyperon puzzle, advance the unified theory of nuclear forces, and quantify QCD

flavor symmetry breaking.

Numerical setup: Calculation presented in this Letter is based on the gauge configurations generated by the CLQCD collaboration with 2+1 dynamical quark flavors, employing the tadpole-improved Symanzik gauge action and Clover fermion action [47]. We use seven ensembles with three lattice spacing values: $a = 0.105$ fm, 0.077 fm and 0.052 fm, and various pion masses ranging from 135 MeV to 317 MeV. The diverse parameters across these ensembles facilitate a robust extrapolation of our results to the physical pion mass and continuum limit. The detailed information regarding these ensembles is provided in Table I.

ID	$a(\text{fm})$	$(L/a)^3 \times T/a$	$m_\pi(\text{MeV})$	N_{conf}
C24P29	0.10530	$24^3 \times 72$	292.7(1.2)	872
C32P29	0.10530	$32^3 \times 64$	292.4(1.1)	984
C48P23	0.10530	$48^3 \times 96$	225.6(0.9)	265
C48P14	0.10530	$48^3 \times 96$	135.5(1.6)	259
F48P21	0.07746	$48^3 \times 96$	207.2(1.1)	220
F48P30	0.07746	$48^3 \times 96$	303.4(0.9)	359
H48P32	0.05187	$48^3 \times 144$	317.2(0.9)	274

TABLE I: Parameters of lattice ensembles: the lattice spacing a , lattice size $(L/a)^3 \times T/a$, the mass of pion m_π and the number of configurations N_{conf} .

Quark propagators are computed using the distillation quark smearing method [48]. The smearing operator is composed of a small number (N_{ev}) of the eigenvectors associated with the N_{ev} lowest eigenvalues of the three-dimensional Laplacian defined in terms of the HYP-smear gauge fields. The number of eigenvectors N_{ev} is 100 for the ensembles with $L/a = 24$ and 32, and 200 for the ensembles with $L/a=48$. Further increases in N_{ev} do not alter the extracted spectrum [49].

Finite-volume spectrum: To obtain the finite-volume spectrum of the $p - \Lambda$ system, we start with the construction of the interpolating operators. In continuum space, the rotational symmetry is described by the group $SU(2)$, its irreducible representations(irreps) are labeled by the total angular momentum $J = 0, 1/2, 1, \dots$. While on the lattice, the rotational symmetry is reduced to the double cover of the cubic group, O^D . Including parity extends this group to $O_h^D = O^D \otimes Z_2$, with Z_2 accounting for the spatial inversion. In moving frames, the symmetry is further reduced to little groups, and operators must be constructed in the irreps of O_h^D and its little groups.

In this work, we study the S-wave $p - \Lambda$ scattering in both 1S_0 and 3S_1 channels, and construct the operators in the rest frame as well as the moving frame with total momentum $\vec{P} = (0, 0, 1)$ (in units of $\frac{2\pi}{L}$). For the 1S_0 channel, the relevant irreps are A_1^+ in the rest frame and A_1 in the moving frame. For the 3S_1 channel, the relevant irreps are T_1^+ in the rest frame and E_2 in the moving frame. The general form of the $p - \Lambda$ operators can be

written as

$$O_{p_1, p_2}^{\Lambda, \lambda, \vec{P}} = \sum_{\mu, \nu, \vec{p}_1, \vec{p}_2} c_{\mu, \nu, \vec{p}_1, \vec{p}_2}^{\Lambda, \lambda, \vec{P}} p_\mu(\vec{p}_1) \Lambda_\nu(\vec{p}_2), \vec{P} = \vec{p}_1 + \vec{p}_2. \quad (1)$$

where p and Λ denote the single-particle operators for proton and Λ , respectively, and μ, ν are spinor indices. Λ labels the irrep and λ denotes its row. The sum runs over all momenta $\vec{p}_1(\vec{p}_2)$ with fixed magnitude $p_1(p_2)$ that are related by the rotations of the cubic group. The coefficients $c_{\mu, \nu, \vec{p}_1, \vec{p}_2}^{\Lambda, \lambda, \vec{P}}$ are chosen so that the operator transforms under the irrep Λ . These coefficients are constructed following the method of Ref. [50] and are computed using the open-source package **OpTion** [50] provided therein. The single particle operators and the explicit form of the $p - \Lambda$ two particle operators are provided in the supplemental materials [60].

To validate a single-channel two-body scattering analysis, we restrict the energy range below the $p - \Sigma$ threshold and the open three-body thresholds (e.g., $p\Lambda\pi$). Accordingly, we use one operator with $p_1 = p_2 = 0$ in the rest frame and two operators in the moving frame $\vec{P} = (0, 0, 1)$: one with $p_1 = 1, p_2 = 0$ and the other one with $p_1 = 0, p_2 = 1$.

The spectrum is extracted from correlation functions of the operators introduced above:

$$C_{ij}(t) = \sum_{t_s} \langle O_i(t + t_s) O_j^\dagger(t_s) \rangle, \quad (2)$$

where i, j index the two-particle operators. In the rest frame, one operator is used. For the moving frame, C is a 2×2 matrix. The source time t_s runs over all time slices to increase statistics.

Solving the generalized eigenvalue problem(GEVP) [51]:

$$C(t)v_n(t, t_0) = \lambda_n(t, t_0)C(t_0)v_n(t, t_0), \quad (3)$$

the energies can be obtained by fitting the eigenvalues $\lambda_n(t, t_0)$ to an exponential form. In practice, we employ the following ratio to subtract the non-interacting energy:

$$\mathcal{R}_n(t, t_0) = \frac{\lambda_n(t, t_0)}{C_p(t - t_0)C_\Lambda(t - t_0)} \xrightarrow{t \rightarrow \infty} A_n e^{-\Delta E_n(t - t_0)}, \quad (4)$$

where C_p and C_Λ are the single-particle correlation functions of the p and Λ at zero momentum, respectively, and ΔE_n is the energy shift relative to threshold:

$$\Delta E_n = E_n - m_p - m_\Lambda. \quad (5)$$

The energy shift ΔE_n is extracted by fitting $\mathcal{R}_n(t, t_0)$ to the form $A_n e^{-\Delta E_n(t - t_0)}$ at a time window where the effective mass exhibits a clear plateau. All fits yield χ^2 per degree of freedom around or less than one. The final results for ΔE_n are summarized in Tab. II. More fitting details are provided in the supplemental materials [60].

	$\vec{P} = (0, 0, 0)$		$\vec{P} = (0, 0, 1)$			
	A_1^+	T_1^+	A_1		E_2	
ΔE (MeV)	ΔE_0	ΔE_0	ΔE_1	ΔE_2	ΔE_1	ΔE_2
C24P29	-28(7)	-21(5)				
C32P29	-19(2)	-9(3)	39(3)	49(3)	47(1)	
C48P23	-4(1)	-3(1)	21(4)	22(2)	18(1)	22(3)
C48P14	-6(2)	-3(2)	-6(4)	18(6)	8(3)	15(2)
F48P30	-6.7(8)	-6(1)	31(2)	40(3)	33(3)	44(4)
F48P21	-7(2)	-9(2)	34(6)	60(7)	31(6)	40(7)
H48P32	-12(3)	-10(2)	69(11)	109(18)	94(10)	123(9)

TABLE II: Results for the energy difference ΔE in unit MeV in the center-of-mass frame $\vec{P} = (0, 0, 0)$ and the moving frame $\vec{P} = (0, 0, 1)$ obtained in our simulations for the ensembles. Note: $\Delta E_n = E_n - (m_p + m_\Lambda)$. Empty entries indicate no reliable extraction due to statistical noise or excited-state contamination.

Scattering analysis: Scattering parameters are determined using Lüscher's finite-volume method [51–53], which connects the finite-volume spectrum with the scattering phase shift in infinite volume. Ignoring the effects of the higher partial wave mixing, Lüscher's formula in all the irreps considered here reduces to:

$$q \cot \delta_0(q) = \frac{1}{\pi^{3/2} \gamma} \mathcal{Z}_{00}^{\mathbf{d}}(1; q^2), \quad (6)$$

where $\mathcal{Z}_{00}^{\mathbf{d}}(1; q^2)$ is the generalized zeta function that can be evaluated numerically for a given q . The dimensionless variable q is defined in terms of the scattering momentum k as $q = kL/2\pi$, and k is related to the center-of-momentum frame energy $E^* = \sqrt{m_1^2 + k^2} + \sqrt{m_2^2 + k^2}$, where $m_{1,2}$ are the masses of the two scattering particles. In a moving frame, the zeta function also depends on the Lorentz factor $\gamma = E/E^*$, with E denoting the energy in the moving frame, and the coefficient $A \equiv 1 + \frac{m_1^2 - m_2^2}{E^{*2}}$, which accounts for the mass difference of the two particles [54]. The detailed expression for the zeta function is provided in the supplemental materials [60].

Near the threshold, the phase shift can be parametrized using the effective range expansion:

$$k^{2l+1} \cot \delta_l(k) = \frac{1}{a_l} + \frac{1}{2} r_l k^2 + \dots, \quad (7)$$

where a_l is the scattering length and r_l is the effective range for partial wave l , and the ellipsis represents terms that are higher order in k^2 .

In this work, we focus on S -wave ($l = 0$) contributions and neglect the mixing effects from D -waves and higher partial waves ($l \geq 2$), which are expected to give only minor corrections to the S -wave observables. We compute the values of $k \cot \delta_0$ using Eq. 6 and obtain the S -wave scattering length a_0 and effective range r_0 by fitting the data to Eq. (7).

As an example, Fig.1 shows the fit for the ensembles with $m_\pi = 292$ MeV and lattice spacing $a = 0.1053$ fm. Fits for the remaining ensembles are provided in the Supplemental Material [60]. The extracted scattering lengths and effective ranges for all ensembles are summarized in Table III.

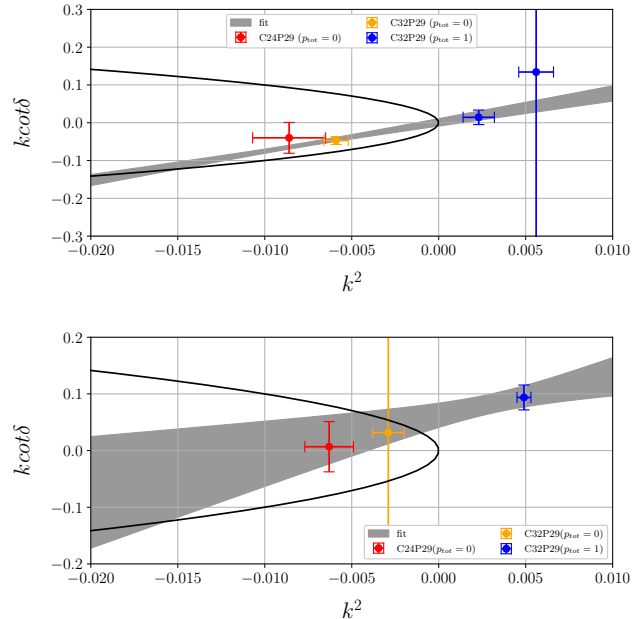


FIG. 1: The values of $k \cot \delta$ as a function of k^2 . The data points are from the ensembles C24P29 and C32P29, having the same pion mass and lattice spacing. The gray bands are the fits to Eq. (7) and the width of the bands indicate 1σ statistical uncertainty. The black curves are ik . The upper and lower panels are for the 1S_0 and 3S_1 channels, respectively.

	1S_0		3S_1	
	a_0^{-1} (GeV)	r_0 (fm)	a_0^{-1} (GeV)	r_0 (fm)
C24P29/C32P29	$0.0002^{+0.0195}_{-0.0156}$	$1.58^{+0.24}_{-0.19}$	$0.110^{+0.034}_{-0.025}$	$1.61^{+0.45}_{-0.74}$
C48P23	$0.077^{+0.056}_{-0.034}$	$1.74^{+2.19}_{-2.85}$	$0.094^{+0.139}_{-0.060}$	$-10.1^{+6.5}_{-18.8}$
C48P14	$0.054^{+0.066}_{-0.034}$	$3.81^{+1.53}_{-0.82}$	$-0.028^{+0.005}_{-0.005}$	$2.89^{+0.55}_{-0.40}$
F48P30	$0.052^{+0.034}_{-0.032}$	$-1.60^{+1.13}_{-1.46}$	$0.106^{+0.053}_{-0.047}$	$-1.40^{+1.48}_{-2.05}$
F48P21	$0.061^{+0.086}_{-0.078}$	$-1.75^{+2.47}_{-4.68}$	$0.017^{+0.059}_{-0.072}$	$-0.87^{+2.08}_{-3.55}$
H48P32	$0.178^{+0.321}_{-0.176}$	$-1.32^{+3.15}_{-6.12}$	$0.201^{+0.190}_{-0.128}$	$-3.68^{+1.20}_{-2.26}$

TABLE III: The fitting result for the 1S_0 -wave and 3S_1 -wave scattering using the ERE parametrization. ERE fit results for the C24P29 and C32P29 ensembles are listed in the first column. The distribution of the 3000 bootstrap replicates exhibits significant non-Gaussian asymmetry. We report the median as the central estimate, with uncertainties corresponding to the 1σ equivalent quantiles for upper and lower bounds.

Chiral and Continuum extrapolation. For both 1S_0

and 3S_1 channels, we extrapolate the inverse of scattering length and the effective range to physical pion mass and continuum limit using the following parametrization [55]:

$$\begin{aligned} a_0^{-1} &= a_{0,\text{phys}}^{-1} + c_1(m_\pi^2 - m_{\pi,\text{phys}}^2) + c_2 a^2, \\ r_0 &= r_{0,\text{phys}} + c_3(m_\pi^2 - m_{\pi,\text{phys}}^2) + c_4 a^2. \end{aligned} \quad (8)$$

For the 1S_0 channel, the extrapolated results are

$$a_{0,\text{phys}}^{-1} = 0.177(83) \text{ GeV}, \quad r_{0,\text{phys}} = 2.9(1.4) \text{ fm}, \quad (9)$$

while the 3S_1 channel, they are

$$a_{0,\text{phys}}^{-1} = 0.016(76) \text{ GeV}, \quad r_{0,\text{phys}} = 1.8(1.1) \text{ fm}. \quad (10)$$

The extrapolations of $1/a_0$ and r_0 for 1S_0 and 3S_1 are shown in Fig. 2 and Fig. 3, respectively.

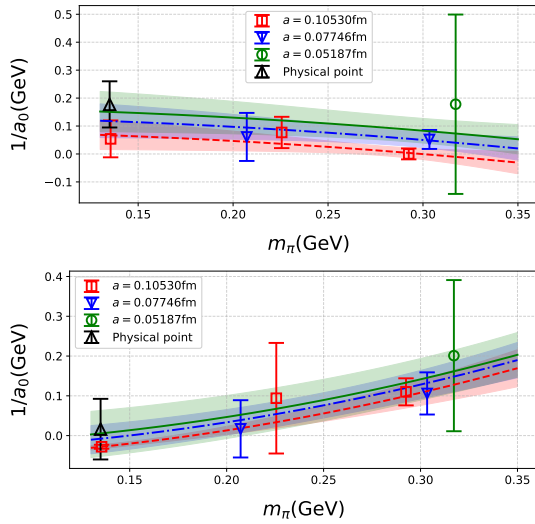


FIG. 2: Results for the $1/a_0$ extrapolation according to Eq. (8) for the channel 1S_0 (upper panel) and 3S_1 (lower panel) with the corresponding $\chi^2/d.o.f = 0.15$ and $\chi^2/d.o.f = 0.18$. The black point corresponds to the physical point and continuum limit.

Discussions: A critical benchmark for our lattice results is direct comparison with experimental data on scattering parameters. The STAR detector at RHIC has provided the spin-averaged experimental values: [18]:

$$a_0 = (2.32_{-0.11}^{+0.12}) \text{ fm}, \quad r_0 = (3.5_{-1.3}^{+2.7}) \text{ fm}. \quad (11)$$

For our lattice results, we perform spin averaging of the 1S_0 and 3S_1 channel parameters, yielding

$$a_{0,\text{avg}} = 3.5(3.8) \text{ fm}, \quad r_{0,\text{avg}} = 2.08(90) \text{ fm}. \quad (12)$$

These values are consistent with the STAR measurements within statistical errors, marking the first direct agreement between lattice QCD predictions and experimental data for $p - \Lambda$ scattering.

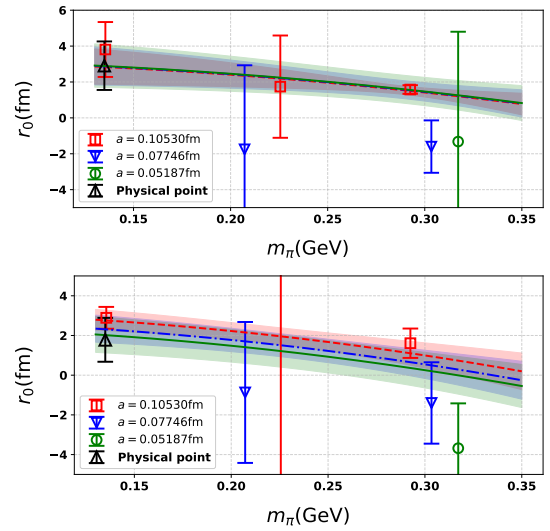


FIG. 3: Results for the r_0 extrapolation according to Eq. (8) for the channel 1S_0 and 3S_1 with the corresponding $\chi^2/d.o.f = 1.2$, and the corresponding $\chi^2/d.o.f = 1.1$. The black point corresponds to the physical point and continuum limit.

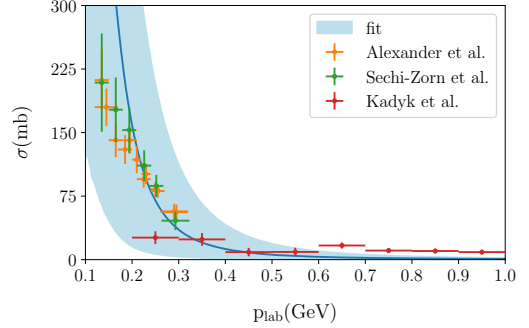


FIG. 4: Comparison of the spin-averaged cross section with experimental measurements [8–10]

Using the extracted s-wave phase shifts and the standard cross-section formula

$$\sigma_l = \frac{4\pi}{k^2} (2l + 1) \sin^2 \delta_l, \quad (13)$$

we compute the spin-averaged s-wave $p - \Lambda$ scattering cross-section and compare it with available experimental data [8–10]. As shown in Fig. 4, our results have a larger central value but still align with experimental measurements within error bars for most momentum ranges. The slight discrepancy at low momenta ($p_{\text{lab}} \leq 0.2 \text{ GeV}$) may stem from two factors: first, the amplified statistical uncertainties near threshold (where small fluctuations in energy levels propagate to $k \cot \delta$ via Lüscher's relation); second, the limited applicability of the single-channel ERE in capturing subtle threshold behaviors of hyperon-nucleon interactions.

The $k \cot \delta - k^2$ plots presented in the previous section show a consistent pattern of attractive interactions across all simulated pion masses. A sufficiently strong attraction can generate poles in the analytically-continued scattering amplitude, which lives on multiple Riemann sheets (RSs) in the complex $s = E_{\text{CM}}^2$ plane. The scattering amplitude with partial wave l and total angular momentum J is proportional to $(k \cot \delta_l^{(J)} - ik)^{-1}$ [52]. The scattering t-matrix can be written as

$$t_l^{(J)} \sim \frac{\sqrt{s}}{2} \frac{1}{k \cot \delta_l^{(J)} - ik}. \quad (14)$$

Positions of poles determine whether the system exhibits a bound state, a virtual state, or a resonance. In particular, the intersection of ERE curve with upper half of the parabola defined by ik indicates a pole below threshold on the real energy axis of the second RS, corresponding to a virtual state.

For the channel 1S_0 , the resulting pole positions extracted from all ensembles used in this work are summarized in Fig. 5, yielding a $p - \Lambda$ mass difference of $-3(18)$ MeV after chiral and continuum extrapolation, consistent with the attractive nature of the $p - \Lambda$ interaction inferred from our scattering parameters. For the channel 3S_1 , reducing the pion mass from 300 MeV toward its physical value induces a continuous migration of the S -matrix pole. The pole trajectory originates on the second Riemann sheet, approaches the threshold, and subsequently moves onto the physical sheet. This evolution suggests that the state, initially virtual at larger m_π , may transition into a bound-state-like pole as the physical point is approached.

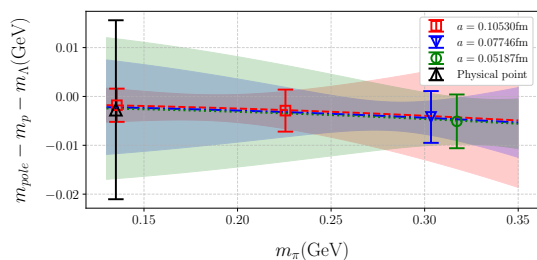


FIG. 5: The $m_{pole} - m_p - m_\Lambda$ of the virtual state for 1S_0 . We performed a joint extrapolation ($m_{pole} = m_{pole,phys} + c_5(m_\pi^2 - m_{\pi,phys}^2) + c_6 a^2$) of the pole trajectory to the physical point. The mass difference at the physical point are $-3(18)$ MeV.

Summary. We have presented a first systematic lattice QCD study of the $p - \Lambda$ scattering based on seven gauge ensembles with $2 + 1$ dynamical flavors at pion masses from 135.5 MeV to 317.2 MeV and of three different lattice spacings. We investigate the $p - \Lambda$ interaction through a systematic analysis of single- and two-particle correlation functions. Utilizing the effective range expansion and incorporating chiral and continuum extrapola-

tions, we find that the $p - \Lambda$ system exhibits weak attractive interactions within the considered energy regime.

Extrapolating to the physical point and the continuum limit, we obtain the inverse of scattering length and effective range for the 1S_0 channel as 0.177(83) GeV and 2.9(1.4) fm. For the 3S_1 channel, we find $1/a_0 = 0.016(76)$ GeV and $r_0 = 1.8(1.1)$ fm. These results are consistent with spin-averaged experimental results.

The next key objective in our study of hyperon-nucleon interactions is a full $p\Lambda - N\Sigma$ coupled-channel analysis [57], as well as the extension to additional channels involving hyperons. The explicit inclusion of a physical ensemble with a smaller lattice spacing in the future may greatly reduce the systematic error.

Acknowledgments. We thank Lie-Wen Chen, Meng-Lin Du, Lisheng Geng, Feng-Kun Guo, Jun He, Y. Hu, Chuan Liu, Tao Luo, Yu Lu, Yan Lyu, Yi-Feng Sun, Jia-Jun Wu, Hanyang Xing, Jun-Ting Ye, and Kang Yu for useful discussions. We thank the CLQCD collaborations for providing us the gauge configurations with dynamical fermions [47], which are generated on the HPC Cluster of ITP-CAS, the Southern Nuclear Science Computing Center(SNSC), the Siyuan-1 cluster supported by the Center for High Performance Computing at Shanghai Jiao Tong University, and the Dongjiang Yuan Intelligent Computing Center. This work is supported in part by National Natural Science Foundation of China under grants No.12125503, 12305103, 12405101, and 124B2096.

Appendix A: Baryon Operators, correlation functions and dispersion relations

For the proton and Λ , both of which have quantum numbers $J^P = \frac{1}{2}^+$, the interpolating operators are:

$$\begin{aligned}\mathcal{O}_p^\mu(\vec{p}, t) &= \sum_{\vec{x}} \epsilon^{abc} [u^{aT}(\vec{x}, t)(C\gamma_5)d^b(\vec{x}, t)](u^c)^\mu(\vec{x}, t)e^{i\vec{p}\cdot\vec{x}} \\ \mathcal{O}_\Lambda^\mu(\vec{p}, t) &= \sum_{\vec{x}} \epsilon^{abc} [u^{aT}(\vec{x}, t)(C\gamma_5)d^b(\vec{x}, t)](s^c)^\mu(\vec{x}, t)e^{i\vec{p}\cdot\vec{x}},\end{aligned}\quad (\text{A1})$$

where \vec{p} and \vec{x} are three-dimensional vectors. For convenient, one can define:

$$\begin{aligned}\mathcal{O}^{m_s=1/2}(\vec{p}, t) &= \mathcal{O}^{\mu=1}(\vec{p}, t), \\ \mathcal{O}^{m_s=-1/2}(\vec{p}, t) &= \mathcal{O}^{\mu=2}(\vec{p}, t),\end{aligned}\quad (\text{A2})$$

where the $\mathcal{O}_{1,2}$ are the upper two components of Dirac four-spinor $\mathcal{O}_{\mu=1,\dots,4}$ in the Dirac basis. The positive-parity is captured by the upper two components of the spinor in the Dirac basis.

The correlation function, with a definite three-momentum \vec{p} , for proton and Λ are defined respectively as:

$$\begin{aligned}C_p(\vec{p}, t) &= \langle \mathcal{O}_p(\vec{p}, t)(\mathcal{O}_p(\vec{p}, 0))^\dagger \rangle \\ C_\Lambda(\vec{p}, t) &= \langle \mathcal{O}_\Lambda(\vec{p}, t)(\mathcal{O}_\Lambda(\vec{p}, 0))^\dagger \rangle.\end{aligned}\quad (\text{A3})$$

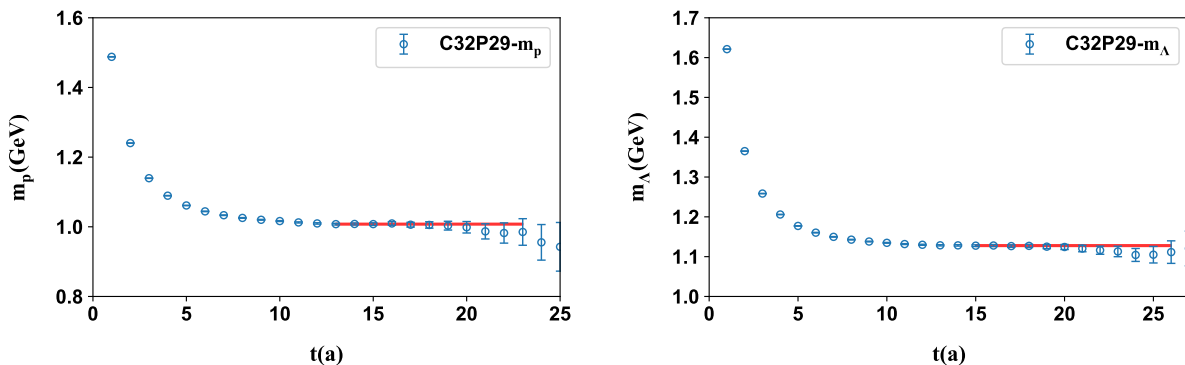


FIG. 6: The ground energies of the proton and Λ on the ensemble C32P29. The horizontal bars indicate the fitted masses and the fit ranges.

To examine the mass-energy dispersion relations of these two baryons and ensure the lattice discretization effects are well-controlled, we generate two-point correlation functions for the proton and Λ baryon at different momenta. From these correlation functions, the baryon energies $E_p(\vec{p})$ and $E_\Lambda(\vec{p})$ for various lattice momenta \vec{p} can be readily obtained. Fig. 7 illustrates the dispersion relation, with the left panel showing the dispersion relation for the proton and the right for Λ on the ensemble C32P29, where five momenta $\vec{p} = [0, 0, 0], [0, 0, 1], [0, 1, 1], [1, 1, 1], [0, 0, 2] \frac{2\pi}{L}$ are chosen. The dispersion relation is then parametrized as follows:

$$E^2 = m^2 + Zp^2. \quad (\text{A4})$$

Here, Z is a parameter determined through fitting. As shown in Fig. 7, all lattice results are well-described by Eq. (A4), yielding a reasonable $\chi^2/\text{d.o.f.} = 0.2$ for proton and $\chi^2/\text{d.o.f.} = 0.71$ for Λ . The values $Z_p = 0.982(16)$ and $Z_\Lambda = 0.985(11)$ are consistent with the square of the speed of light.

Appendix B: Two-baryon operators and correlation functions

For two-baryon states, the operators must encode the system's relevant symmetries, including relative spatial separation and total angular momentum, to accurately describe interparticle interactions. Constructing such two-particle operators further demands careful accounting of relevant internal quantum numbers. On the lattice, the

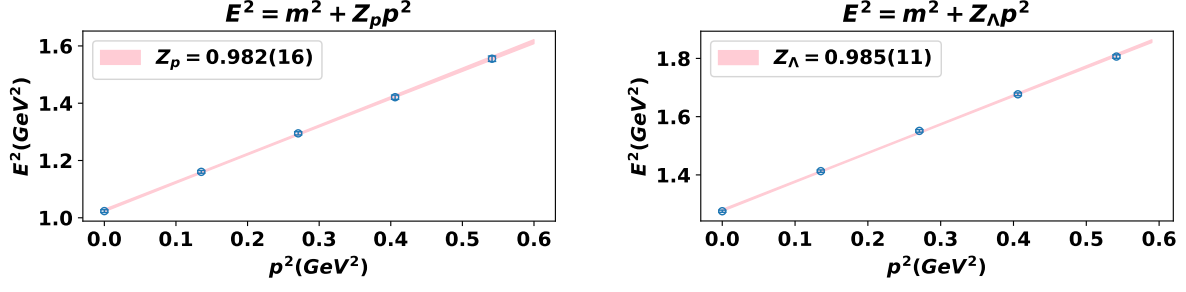


FIG. 7: Dispersion relation for proton (upper panel) and for Λ on the C32P29 ensembles (lower panel).

continuous rotational symmetry group $SO(3)$ is broken to the corresponding discrete point group. Here, we focus on the 1S_0 and 3S_1 channels, which correspond to the irreps A_1^+ and T_1^+ (respectively) in the center-of-mass frame, and utilize the publicly available `OpTion` package [50] to perform group-theoretic projection.

The corresponding correlation matrix are constructed as:

$$C_{ij}(t, t_s) = \langle \mathcal{O}_i(t) \mathcal{O}_j^\dagger(t_s) \rangle, \quad (\text{B1})$$

where \mathcal{O}_i represents the two-particle operator defined in Eq.(B5), and i and j can take values 1 or 2. The two-particle energies, which are substituted into Lüscher's formula, are extracted from this correlation matrix by solving the generalized eigenvalue problem (GEVP):

$$C(t) \cdot v_n(t, t_0) = \lambda_n(t, t_0) C(t_0) \cdot v_n(t, t_0), \quad (\text{B2})$$

with $n = 1, 2, \dots, N$ and $t > t_0$. The eigenvalues $\lambda_n(t, t_0)$ can be shown to behave like

$$\lambda_n \simeq e^{-E_n(t-t_0)} (1 + C_1 e^{-\Delta E(t-t_0)}). \quad (\text{B3})$$

The finite-volume energy eigenvalues E_n are extracted from the correlation matrix and mapped to the interacting momentum q^2 , which serves as the input for Lüscher's formula to determine scattering parameters. The reference time t_0 is optimized to suppress excited-state contamination while maintaining a sufficient signal-to-noise ratio.

1. Two-particle operators Constructing in the center-of-mass frame

In this work, the publicly available package `OpTion` [50] is utilized to construct the group theory projection. The scattering analysis is restricted to the A_1^+ (1S_0) and T_1^+ (3S_1) irreps of the cubic group (O_h) at rest:

$$\begin{aligned}
& A_1^+ : \\
& \mathcal{O}_{A_1^+}^1 = \mathcal{O}_{\mu=\frac{1}{2}}^p(\vec{0}, t) \mathcal{O}_{\mu=-\frac{1}{2}}^\Lambda(\vec{0}, t) - \mathcal{O}_{\mu=-\frac{1}{2}}^p(\vec{0}, t) \mathcal{O}_{\mu=\frac{1}{2}}^\Lambda(\vec{0}, t) \\
& \mathcal{O}_{A_1^+}^2 = \mathcal{O}_{\mu=\frac{1}{2}}^p(\vec{e}_x, t) \mathcal{O}_{\mu=-\frac{1}{2}}^\Lambda(-\vec{e}_x, t) - \mathcal{O}_{\mu=-\frac{1}{2}}^p(\vec{e}_x, t) \mathcal{O}_{\mu=\frac{1}{2}}^\Lambda(-\vec{e}_x, t) \\
& \quad + \mathcal{O}_{\mu=\frac{1}{2}}^p(-\vec{e}_x, t) \mathcal{O}_{\mu=-\frac{1}{2}}^\Lambda(\vec{e}_x, t) - \mathcal{O}_{\mu=-\frac{1}{2}}^p(-\vec{e}_x, t) \mathcal{O}_{\mu=\frac{1}{2}}^\Lambda(\vec{e}_x, t) \\
& \quad + \mathcal{O}_{\mu=\frac{1}{2}}^p(\vec{e}_y, t) \mathcal{O}_{\mu=-\frac{1}{2}}^\Lambda(-\vec{e}_y, t) - \mathcal{O}_{\mu=-\frac{1}{2}}^p(\vec{e}_y, t) \mathcal{O}_{\mu=\frac{1}{2}}^\Lambda(-\vec{e}_y, t) \\
& \quad + \mathcal{O}_{\mu=\frac{1}{2}}^p(-\vec{e}_y, t) \mathcal{O}_{\mu=-\frac{1}{2}}^\Lambda(\vec{e}_y, t) - \mathcal{O}_{\mu=-\frac{1}{2}}^p(-\vec{e}_y, t) \mathcal{O}_{\mu=\frac{1}{2}}^\Lambda(\vec{e}_y, t) \\
& \quad + \mathcal{O}_{\mu=\frac{1}{2}}^p(\vec{e}_z, t) \mathcal{O}_{\mu=-\frac{1}{2}}^\Lambda(-\vec{e}_z, t) - \mathcal{O}_{\mu=-\frac{1}{2}}^p(\vec{e}_z, t) \mathcal{O}_{\mu=\frac{1}{2}}^\Lambda(-\vec{e}_z, t) \\
& \quad + \mathcal{O}_{\mu=\frac{1}{2}}^p(-\vec{e}_z, t) \mathcal{O}_{\mu=-\frac{1}{2}}^\Lambda(\vec{e}_z, t) - \mathcal{O}_{\mu=-\frac{1}{2}}^p(-\vec{e}_z, t) \mathcal{O}_{\mu=\frac{1}{2}}^\Lambda(\vec{e}_z, t), \\
& T_1^+ : \\
& \mathcal{O}_{T_1^+}^1 = \mathcal{O}_{\mu=-\frac{1}{2}}^p(\vec{0}, t) \mathcal{O}_{\mu=-\frac{1}{2}}^\Lambda(\vec{0}, t) - \mathcal{O}_{\mu=\frac{1}{2}}^p(\vec{0}, t) \mathcal{O}_{\mu=\frac{1}{2}}^\Lambda(\vec{0}, t)
\end{aligned} \quad (\text{B4})$$

$$\begin{aligned}
\mathcal{O}_{T_1^+}^2 &= \mathcal{O}_{\mu=-\frac{1}{2}}^P(\vec{e}_x, t)\mathcal{O}_{\mu=-\frac{1}{2}}^\Lambda(-\vec{e}_x, t) - \mathcal{O}_{\mu=\frac{1}{2}}^P(\vec{e}_x, t)\mathcal{O}_{\mu=\frac{1}{2}}^\Lambda(-\vec{e}_x, t) \\
&+ \mathcal{O}_{\mu=-\frac{1}{2}}^P(-\vec{e}_x, t)\mathcal{O}_{\mu=-\frac{1}{2}}^\Lambda(\vec{e}_x, t) - \mathcal{O}_{\mu=\frac{1}{2}}^P(-\vec{e}_x, t)\mathcal{O}_{\mu=\frac{1}{2}}^\Lambda(\vec{e}_x, t) \\
&+ \mathcal{O}_{\mu=-\frac{1}{2}}^P(\vec{e}_y, t)\mathcal{O}_{\mu=-\frac{1}{2}}^\Lambda(-\vec{e}_y, t) - \mathcal{O}_{\mu=\frac{1}{2}}^P(\vec{e}_y, t)\mathcal{O}_{\mu=\frac{1}{2}}^\Lambda(-\vec{e}_y, t) \\
&+ \mathcal{O}_{\mu=-\frac{1}{2}}^P(-\vec{e}_y, t)\mathcal{O}_{\mu=-\frac{1}{2}}^\Lambda(\vec{e}_y, t) - \mathcal{O}_{\mu=\frac{1}{2}}^P(-\vec{e}_y, t)\mathcal{O}_{\mu=\frac{1}{2}}^\Lambda(\vec{e}_y, t) \\
&+ \mathcal{O}_{\mu=-\frac{1}{2}}^P(\vec{e}_z, t)\mathcal{O}_{\mu=-\frac{1}{2}}^\Lambda(-\vec{e}_z, t) - \mathcal{O}_{\mu=\frac{1}{2}}^P(\vec{e}_z, t)\mathcal{O}_{\mu=\frac{1}{2}}^\Lambda(-\vec{e}_z, t) \\
&+ \mathcal{O}_{\mu=-\frac{1}{2}}^P(-\vec{e}_z, t)\mathcal{O}_{\mu=-\frac{1}{2}}^\Lambda(\vec{e}_z, t) - \mathcal{O}_{\mu=\frac{1}{2}}^P(-\vec{e}_z, t)\mathcal{O}_{\mu=\frac{1}{2}}^\Lambda(\vec{e}_z, t).
\end{aligned} \tag{B5}$$

2. Two particles scattering in moving frames in a finite volume

There are two particles with total three-momentum \mathbf{P} in a box, and the total momentum satisfies

$$\mathbf{P} = \mathbf{p}_1 + \mathbf{p}_2 = \frac{2\pi}{L}\mathbf{d}, \mathbf{d} \in Z^3. \tag{B6}$$

Then the energy E^* is

$$E^{*2} = E_{MF}^2 - \mathbf{P}^2. \tag{B7}$$

In the moving frame, the center-of-mass E^* is moving with a velocity of $v = \mathbf{P}/E_{MF}$ and the Lorentz factor $\gamma = (1 - v^2)^{-1/2}$. To get more eigen-energies near the threshold, we implement the moving frame $d = e_3$. Considering the two particles with different masses, a 2×2 correlation function matrix can be constructed, simulated, and diagonalized to yield the eigen-energies. We focus on the 1S_0 and 3S_1 channels, which correspond to the irreps A_1 and E_2 in this moving frame, respectively:

$$\begin{aligned}
A_1 : \\
\mathcal{O}_{A_1}^1 &= \mathcal{O}_{\mu=\frac{1}{2}}^P(\vec{0}, t)\mathcal{O}_{\mu=-\frac{1}{2}}^\Lambda(\vec{e}_z, t) - \mathcal{O}_{\mu=-\frac{1}{2}}^P(\vec{0}, t)\mathcal{O}_{\mu=\frac{1}{2}}^\Lambda(\vec{e}_z, t), \\
\mathcal{O}_{A_1}^2 &= \mathcal{O}_{\mu=\frac{1}{2}}^P(\vec{e}_z, t)\mathcal{O}_{\mu=-\frac{1}{2}}^\Lambda(\vec{0}, t) - \mathcal{O}_{\mu=-\frac{1}{2}}^P(\vec{e}_z, t)\mathcal{O}_{\mu=\frac{1}{2}}^\Lambda(\vec{0}, t), \\
E_2 : \\
\mathcal{O}_{E_2}^1 &= \mathcal{O}_{\mu=-\frac{1}{2}}^P(\vec{0}, t)\mathcal{O}_{\mu=-\frac{1}{2}}^\Lambda(\vec{e}_z, t) + \mathcal{O}_{\mu=\frac{1}{2}}^P(\vec{0}, t)\mathcal{O}_{\mu=\frac{1}{2}}^\Lambda(\vec{e}_z, t), \\
\mathcal{O}_{E_2}^2 &= \mathcal{O}_{\mu=-\frac{1}{2}}^P(\vec{e}_z, t)\mathcal{O}_{\mu=-\frac{1}{2}}^\Lambda(\vec{0}, t) + \mathcal{O}_{\mu=\frac{1}{2}}^P(\vec{e}_z, t)\mathcal{O}_{\mu=\frac{1}{2}}^\Lambda(\vec{0}, t).
\end{aligned} \tag{B8}$$

Then the scattering phase shifts can be gained from the total energy of the two-particle system enveloped in a cubic torus by Lüscher technique [51–53, 58]

$$q \cot \delta_0(q) = \frac{1}{\gamma\pi^{3/2}}\mathcal{Z}_{00}^d(1; q^2). \tag{B9}$$

The zeta function $\mathcal{Z}_{00}^d(1; q^2)$ is computed using the expression [59]:

$$\begin{aligned}
\mathcal{Z}_{LM}^d(1; q^2) &= \sum_{\mathbf{r} \in P_d} \frac{e^{-\Lambda(|\mathbf{r}|^2 - q^2)}}{|\mathbf{r}|^2 - q^2} |\mathbf{r}|^L Y_{LM}(\Omega_{\mathbf{r}}) \\
&+ \delta_{L,0} Y_{00} \gamma \pi^{3/2} \left[2q^2 \int_0^\Lambda dt \frac{e^{tq^2}}{\sqrt{t}} - \frac{2}{\sqrt{\Lambda}} e^{\Lambda q^2} \right] \\
&+ \gamma \sum_{\mathbf{w} \neq \mathbf{0}} e^{-i\pi\mathbf{w} \cdot \mathbf{A}\mathbf{d}} |\hat{\gamma}\mathbf{w}|^L Y_{LM}(\Omega_{\hat{\gamma}\mathbf{w}}) \int_0^\Lambda dt \left(\frac{\pi}{t}\right)^{3/2+L} e^{tq^2} e^{-\frac{\pi^2|\hat{\gamma}\mathbf{w}|^2}{t}},
\end{aligned} \tag{B10}$$

where Y_{LM} are spherical harmonics. The factor A accounts for the mass difference of the two scattering particles and is defined as $A = 1 + \frac{m_1^2 - m_2^2}{E^{*2}}$. The sum of \mathbf{r} runs over the set P_d defined by $P_d = \{\mathbf{r} | \mathbf{r} = \hat{\gamma}^{-1}(\mathbf{n} - \frac{1}{2}\mathbf{A}\mathbf{d}), \mathbf{n} \in Z^3\}$. The value of above expression is independent of the choice of the cutoff parameter Λ . In this work, we set $\Lambda = 1$.

Appendix C: The two-particle spectrum

We show the results for the two-particle spectrum in Fig. 8, 9, 10, 11.

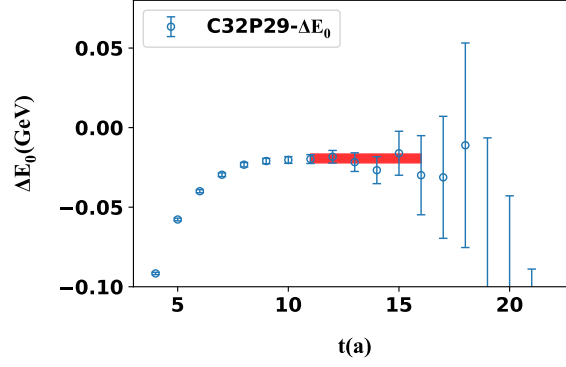


FIG. 8: Effective energy splitting $\Delta E_\alpha = \log \frac{\mathcal{R}_\alpha(t+1, t_0)}{\mathcal{R}_\alpha(t, t_0)}$ for the irrep A_1^+ on the ensemble C32P29 in the center-of-mass frame. The horizontal bars indicate the fitted ΔE_α and the fit ranges.

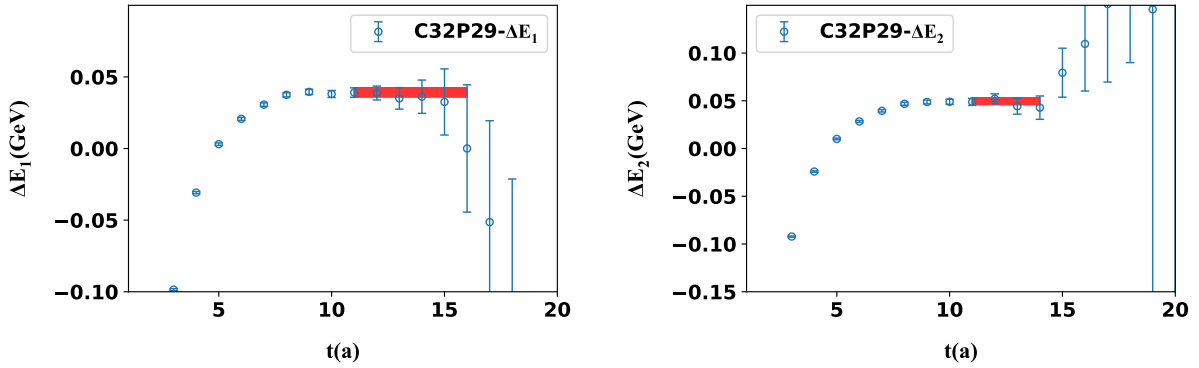


FIG. 9: The two Effective energy splittings for the irrep A_1 on the ensemble C32P29 in the moving frame $d = e_3$. The horizontal bars indicate the fitted ΔE_α and the fit ranges.

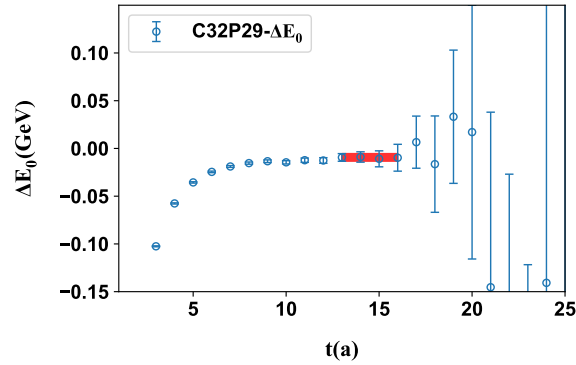


FIG. 10: Effective energy splitting $\Delta E_\alpha = \log \frac{\mathcal{R}_\alpha(t+1, t_0)}{\mathcal{R}_\alpha(t, t_0)}$ for the irrep T_1^+ on the ensemble C32P29 in the center-of-mass frame. The horizontal bars indicate the fitted ΔE_α and the fit ranges.

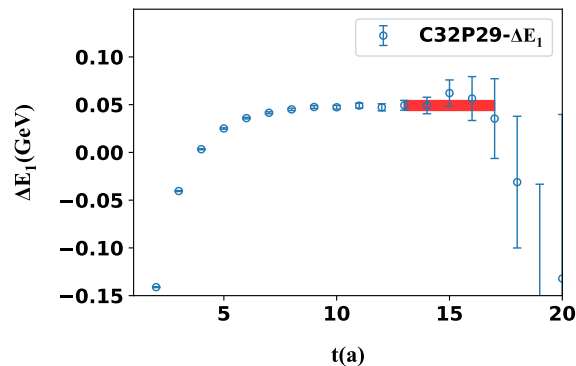


FIG. 11: The Effective energy splitting for the irrep E_2 on the ensemble C32P29 in the moving frame $d = e_3$. The horizontal bars indicate the fitted ΔE_α and the fit ranges.

Appendix D: ERE expansion diagrams of other ensembles

We show the results for ERE expansion diagrams of other ensembles in Fig. 12, and Fig. 13. In Fig. 12, results for the parameter fits according to Eq. (7) for the channel 1S_0 are given. The points are from lattice data from the coresponding ensemble. Both horizontal and vertical coordinates are expressed in lattice units. The gray band corresponds to statistical error. Intersection of the ik curve (black) and the gray band indicates the allowed pole range. Results for the 3S_1 channel are given in Fig. 13.

-
- [1] H. Polinder, J. Haidenbauer and U. G. Meissner, Nucl. Phys. A **779**, 244-266 (2006) doi:10.1016/j.nuclphysa.2006.09.006 [arXiv:nucl-th/0605050 [nucl-th]].
 - [2] L. Tolos and L. Fabbietti, Prog. Part. Nucl. Phys. **112**, 103770 (2020) doi:10.1016/j.pnpnp.2020.103770 [arXiv:2002.09223 [nucl-ex]].
 - [3] I. Vidaña, Proc. Roy. Soc. Lond. A **474**, 0145 (2018) doi:10.1098/rspa.2018.0145 [arXiv:1803.00504 [nucl-th]].
 - [4] I. Vidaña, Nucl. Phys. A **914**, 367-376 (2013) doi:10.1016/j.nuclphysa.2013.01.015
 - [5] B. P. Abbott *et al.* [LIGO Scientific and Virgo], Phys. Rev. Lett. **121**, no.16, 161101 (2018) doi:10.1103/PhysRevLett.121.161101 [arXiv:1805.11581 [gr-qc]].
 - [6] D. Lonardonì, A. Lovato, S. Gandolfi and F. Pederiva, Phys. Rev. Lett. **114**, no.9, 092301 (2015) doi:10.1103/PhysRevLett.114.092301 [arXiv:1407.4448 [nucl-th]].
 - [7] A. Gal, E. V. Hungerford and D. J. Millener, Rev. Mod. Phys. **88**, no.3, 035004 (2016) doi:10.1103/RevModPhys.88.035004 [arXiv:1605.00557 [nucl-th]].
 - [8] G. Alexander, U. Karshon, A. Shapira, G. Yekutieli, R. Engelmann, H. Filthuth and W. Lughofer, Phys. Rev. **173**, 1452-1460 (1968) doi:10.1103/PhysRev.173.1452
 - [9] J. A. Kadyk, G. Alexander, J. H. Chan, P. Gaposchkin and G. H. Trilling, Nucl. Phys. B **27**, 13-22 (1971) doi:10.1016/0550-3213(71)90076-9
 - [10] B. Sechi-Zorn, B. Kehoe, J. Twitty and R. A. Burnstein, Phys. Rev. **175**, 1735-1740 (1968) doi:10.1103/PhysRev.175.1735
 - [11] J. M. Hauptman, J. A. Kadyk and G. H. Trilling, Nucl. Phys. B **125**, 29-51 (1977) doi:10.1016/0550-3213(77)90222-X
 - [12] D. Bassano, C. Y. Chang, M. Goldberg, T. Kikuchi and J. Leitner, Phys. Rev. **160**, no.5, 1239 (1967) doi:10.1103/PhysRev.160.1239
 - [13] G. R. Charlton, J. Badier, E. Barrelet, I. Makarovisch, J. Pernegr, J. R. Hubbard, A. Leveque, C. Louedec, L. Moscoso and D. Revel, Phys. Lett. B **32**, 720-722 (1970) doi:10.1016/0370-2693(70)90454-5
 - [14] K. J. Anderson, N. M. Gelfand, J. Keren and T. H. Tan, Phys. Rev. D **11**, 473-477 (1975) [erratum: Phys. Rev. D **11**, 3359 (1975)] doi:10.1103/PhysRevD.11.473
 - [15] R. P. Mount, R. E. Ansorge, J. R. Carter, W. W. Neale, J. G. Rushbrooke and D. R. Ward, Phys. Lett. B **58**, 228-232 (1975) doi:10.1016/0370-2693(75)90642-5
 - [16] J. Rowley *et al.* [CLAS], Phys. Rev. Lett. **127**, no.27, 272303 (2021) doi:10.1103/PhysRevLett.127.272303 [arXiv:2108.03134 [hep-ex]].
 - [17] M. Ablikim *et al.* [BESIII], Phys. Rev. Lett. **132**, no.23, 231902 (2024) doi:10.1103/PhysRevLett.132.231902 [arXiv:2401.09012 [hep-ex]].
 - [18] Y. Hu [STAR], EPJ Web Conf. **296**, 14010 (2024) doi:10.1051/epjconf/202429614010 [arXiv:2401.00319 [nucl-ex]].
 - [19] T. A. Rijken, V. G. J. Stoks and Y. Yamamoto, Phys. Rev. C **59**, 21-40 (1999) doi:10.1103/PhysRevC.59.21 [arXiv:nucl-th/9807082 [nucl-th]].

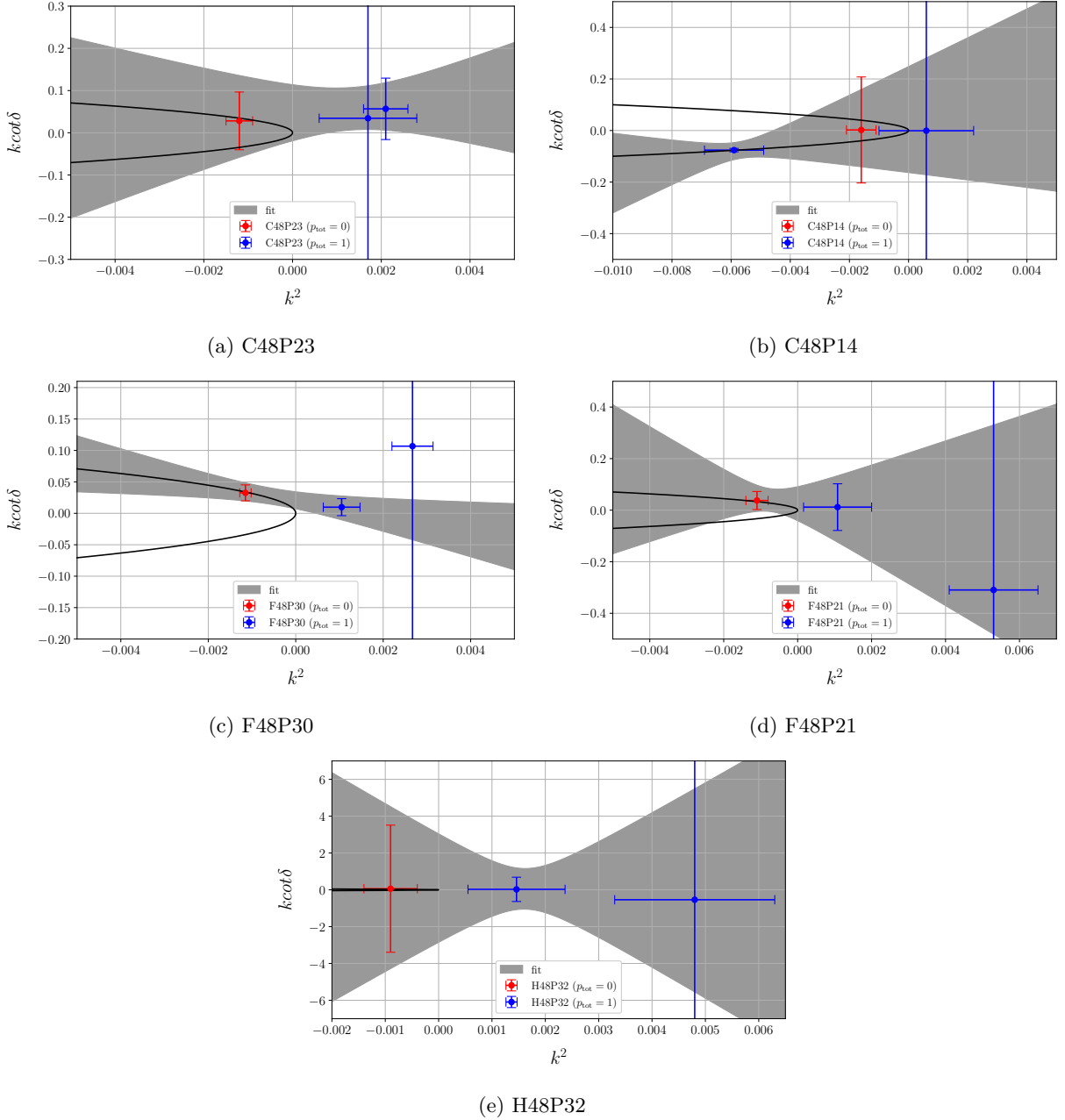


FIG. 12: Results for the parameter fits according to Eq. (7) for the channel 1S_0 . The points are from lattice data from the coresponding ensemble. Both horizontal and vertical coordinates are expressed in lattice units. The gray band corresponds to statistical error. Intersection of the ik curve (black) and the gray band indicates the allowed pole range.

- [20] B. Holzenkamp, K. Holinde and J. Speth, Nucl. Phys. A **500**, 485-528 (1989) doi:10.1016/0375-9474(89)90223-6
- [21] A. Reuber, K. Holinde and J. Speth, Czech. J. Phys. **42**, 1115-1135 (1992) doi:10.1007/BF01591397
- [22] J. Haidenbauer and U. G. Meissner, Phys. Rev. C **72**, 044005 (2005) doi:10.1103/PhysRevC.72.044005 [arXiv:nucl-th/0506019 [nucl-th]].
- [23] M. M. Nagels, T. A. Rijken and J. J. de Swart, Phys. Rev. D **17**, 768 (1978) doi:10.1103/PhysRevD.17.768
- [24] P. M. M. Maessen, T. A. Rijken and J. J. de Swart, Phys. Rev. C **40**, 2226-2245 (1989) doi:10.1103/PhysRevC.40.2226
- [25] T. A. Rijken, M. M. Nagels and Y. Yamamoto, Prog. Theor. Phys. Suppl. **185**, 14-71 (2010) doi:10.1143/PTPS.185.14
- [26] K. Tominaga and T. Ueda, Nucl. Phys. A **693**, 731-754 (2001) doi:10.1016/S0375-9474(01)00882-X
- [27] Z. Y. Zhang, Y. W. Yu, P. N. Shen, L. R. Dai, A. Faessler and U. Straub, Nucl. Phys. A **625**, 59-70 (1997) doi:10.1016/S0375-9474(97)00033-X

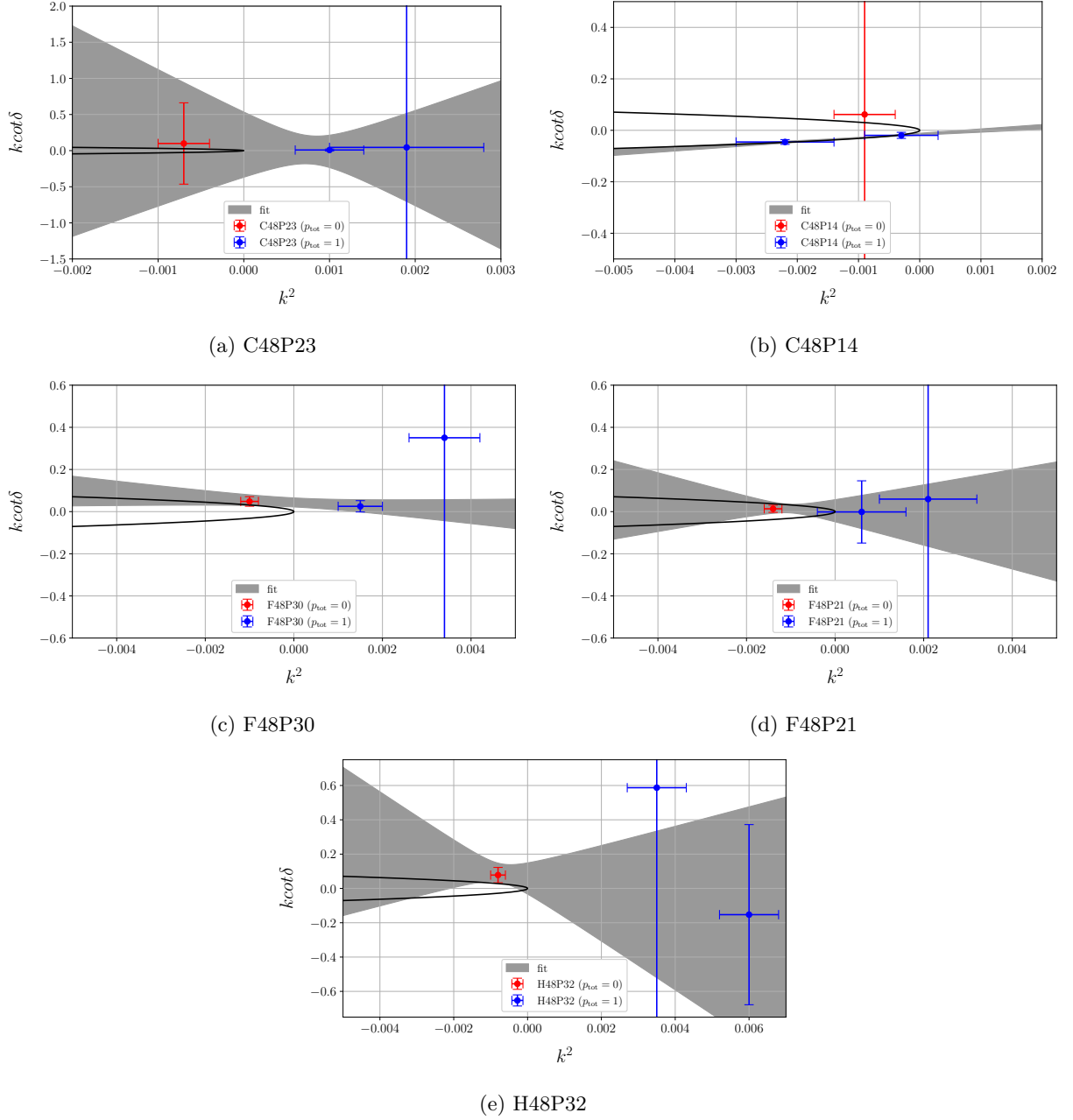


FIG. 13: Results for the parameter fits according to Eq. (7) for the channel 3S_1 . The gray band corresponds to statistical error.

- [28] Y. Fujiwara, Y. Suzuki and C. Nakamoto, Prog. Part. Nucl. Phys. **58**, 439-520 (2007) doi:10.1016/j.pnpnp.2006.08.001 [arXiv:nucl-th/0607013 [nucl-th]].
- [29] Y. Chen and J. He, Phys. Lett. B **871**, 140004 (2025) doi:10.1016/j.physletb.2025.140004 [arXiv:2507.18415 [hep-ph]].
- [30] J. Haidenbauer, S. Petschauer, N. Kaiser, U. G. Meissner, A. Nogga and W. Weise, Nucl. Phys. A **915**, 24-58 (2013) doi:10.1016/j.nuclphysa.2013.06.008 [arXiv:1304.5339 [nucl-th]].
- [31] K. W. Li, X. L. Ren, L. S. Geng and B. Long, Phys. Rev. D **94**, no.1, 014029 (2016) doi:10.1103/PhysRevD.94.014029 [arXiv:1603.07802 [hep-ph]].
- [32] K. W. Li, X. L. Ren, L. S. Geng and B. W. Long, Chin. Phys. C **42**, no.1, 014105 (2018) doi:10.1088/1674-1137/42/1/014105 [arXiv:1612.08482 [nucl-th]].
- [33] J. Haidenbauer, U. G. Meißner and A. Nogga, Eur. Phys. J. A **56**, no.3, 91 (2020) doi:10.1140/epja/s10050-020-00100-4 [arXiv:1906.11681 [nucl-th]].
- [34] J. Song, Z. W. Liu, K. W. Li and L. S. Geng, Phys. Rev. C **105**, no.3, 035203 (2022) doi:10.1103/PhysRevC.105.035203 [arXiv:2107.04742]

- [nucl-th]].
- [35] J. Haidenbauer, U. G. Meißner, A. Nogga and H. Le, *Eur. Phys. J. A* **59**, no.3, 63 (2023) doi:10.1140/epja/s10050-023-00960-6 [arXiv:2301.00722 [nucl-th]].
- [36] K. Miwa *et al.* [J-PARC E40], *Phys. Rev. C* **104**, no.4, 045204 (2021) doi:10.1103/PhysRevC.104.045204 [arXiv:2104.13608 [nucl-ex]].
- [37] S. Muroya, A. Nakamura and J. Nagata, *Nucl. Phys. B Proc. Suppl.* **129**, 239-241 (2004) doi:10.1016/S0920-5632(03)02542-8
- [38] S. R. Beane *et al.* [NPLQCD], *Nucl. Phys. A* **794**, 62-72 (2007) doi:10.1016/j.nuclphysa.2007.07.006 [arXiv:hep-lat/0612026 [hep-lat]].
- [39] N. Ishii, S. Aoki and T. Hatsuda, *Phys. Rev. Lett.* **99**, 022001 (2007) doi:10.1103/PhysRevLett.99.022001 [arXiv:nucl-th/0611096 [nucl-th]].
- [40] N. Ishii *et al.* [HAL QCD], *Phys. Lett. B* **712**, 437-441 (2012) doi:10.1016/j.physletb.2012.04.076 [arXiv:1203.3642 [hep-lat]].
- [41] S. R. Beane, W. Detmold, K. Orginos and M. J. Savage, *Prog. Part. Nucl. Phys.* **66**, 1-40 (2011) doi:10.1016/j.pnpnp.2010.08.002 [arXiv:1004.2935 [hep-lat]].
- [42] H. Nemura, S. Aoki, T. Doi, S. Gongyo, T. Hatsuda, Y. Ikeda, T. Inoue, T. Iritani, N. Ishii and T. Miyamoto, *et al.* PoS **LATTICE2016**, 101 (2017) doi:10.22323/1.256.0101 [arXiv:1702.00734 [hep-lat]].
- [43] H. Nemura, S. Aoki, T. Doi, S. Gongyo, T. Hatsuda, Y. Ikeda, T. Inoue, T. Iritani, N. Ishii and T. Miyamoto, *et al.* EPJ Web Conf. **175**, 05030 (2018) doi:10.1051/epjconf/201817505030 [arXiv:1711.07003 [hep-lat]].
- [44] H. Nemura [LATTICE-HALQCD], *AIP Conf. Proc.* **2130**, no.1, 040005 (2019) doi:10.1063/1.5118402 [arXiv:1810.04046 [hep-lat]].
- [45] J. T. Ye, R. Wang, S. P. Wang and L. W. Chen, *Astrophys. J.* **985**, no.2, 238 (2025) doi:10.3847/1538-4357/add017 [arXiv:2411.18349 [nucl-th]].
- [46] D. Chatterjee and I. Vidaña, *Eur. Phys. J. A* **52**, no.2, 29 (2016) doi:10.1140/epja/i2016-16029-x [arXiv:1510.06306 [nucl-th]].
- [47] Z. C. Hu *et al.* [CLQCD], *Phys. Rev. D* **109**, no.5, 054507 (2024) doi:10.1103/PhysRevD.109.054507 [arXiv:2310.00814 [hep-lat]].
- [48] M. Peardon *et al.* [Hadron Spectrum], *Phys. Rev. D* **80**, 054506 (2009) doi:10.1103/PhysRevD.80.054506 [arXiv:0905.2160 [hep-lat]].
- [49] C. Chen, H. Dong, L. Liu, P. Sun, X. Xiong, Y. B. Yang, F. Yao, J. H. Zhang, C. Zeng and S. Zhong, [arXiv:2510.26425 [hep-lat]].
- [50] H. Yan, C. Liu, L. Liu and Y. Meng, *JHEP* **10**, 210 (2025) doi:10.1007/JHEP10(2025)210 [arXiv:2507.16070 [hep-lat]].
- [51] M. Luscher and U. Wolff, *Nucl. Phys. B* **339**, 222-252 (1990) doi:10.1016/0550-3213(90)90540-T
- [52] M. Luscher, *Commun. Math. Phys.* **105**, 153-188 (1986) doi:10.1007/BF01211097
- [53] M. Luscher, *Nucl. Phys. B* **354**, 531-578 (1991) doi:10.1016/0550-3213(91)90366-6
- [54] L. Leskovec and S. Prelovsek, *Phys. Rev. D* **85**, 114507 (2012) doi:10.1103/PhysRevD.85.114507 [arXiv:1202.2145 [hep-lat]].
- [55] H. Yan, C. Liu, L. Liu, Y. Meng and H. Xing, *Phys. Rev. D* **111**, no.1, 014503 (2025) doi:10.1103/PhysRevD.111.014503 [arXiv:2404.13479 [hep-lat]].
- [56] J. Dai, H. B. Li, H. Miao and J. Zhang, *Chin. Phys. C* **48**, no.7, 073003 (2024) doi:10.1088/1674-1137/ad3dde [arXiv:2209.12601 [hep-ex]].
- [57] S. Acharya *et al.* [ALICE], *Phys. Lett. B* **833**, 137272 (2022) doi:10.1016/j.physletb.2022.137272 [arXiv:2104.04427 [nucl-ex]].
- [58] K. Rummukainen and S. A. Gottlieb, *Nucl. Phys. B* **450**, 397-436 (1995) doi:10.1016/0550-3213(95)00313-H [arXiv:hep-lat/9503028 [hep-lat]].
- [59] S. R. Beane *et al.* [NPLQCD], *Phys. Rev. D* **85**, 034505 (2012) doi:10.1103/PhysRevD.85.034505 [arXiv:1107.5023 [hep-lat]].
- [60] *Supplemental Material for this Article.*